ChemPubSoc Europe

DOI: 10.1002/chem.201503203

CHEMISTRY A European Journal Full Paper

Chemical Biology |*Hot Paper*|

Ruthenium Complex "Light Switches" that are Selective for Different G-Quadruplex Structures

Erin Wachter, Diego Moyá, Sean Parkin, and Edith C. Glazer*[a]

Abstract: Recognition and regulation of G-quadruplex nucleic acid structures is an important goal for the development of chemical tools and medicinal agents. The addition of a bromo-substituent to the dipyridylphenazine (dppz) ligands in the photophysical "light switch", $[Ru(bpy)_2dppz]^{2+}$, and the photochemical "light switch", $[Ru(bpy)_2dmdppz]^{2+}$, creates compounds with increased selectivity for an intermolecular parallel G-quadruplex and the mixed-hybrid G-quadruplex, respectively. When $[Ru(bpy)_2dppz\text{-}Br]^{2+}$ and $[Ru(bpy)_2dmdppz\text{-}Br]^{2+}$ are incubated with the G-quadruplexes, they have a stabilizing effect on the DNA structures. Activation of $[Ru(bpy)_2dmdppz\text{-}Br]^{2+}$ with light results in covalent adduct formation with the DNA. These complexes demonstrate that subtle chemical modifications of Ru^{II} complexes can alter G-quadruplex selectivity, and could be useful for the rational design of in vivo G-quadruplex probes.

Introduction

Guanosine-rich (G-rich) regions capable of forming G-quadruplex structures are abundant in the human genome, and their presence in telomeres and promoter regions makes them appealing therapeutic targets.[1] Many proto-oncogenes have G-quadruplex forming regions within their promoter sequence, such as *c-myc*,[2] *c-kit*,[3] and *bcl-2*,[4] and agents that bind the G-quadruplex could affect regulation of gene transcription. G-rich regions are also present at the ends of telomeres that have the ability to form G-quadruplexes, and stabilization of these G-quadruplexes inhibits the ability of the enzyme telomerase to lengthen the telomeres.[5] As a result, the identification of small molecules that demonstrate selectivity for biologically relevant G-quadruplexes is an active area in drug discovery.[1c]

G-quadruplex binding ligands are generally comprised of polyaromatic systems in order to take advantage of the large π surface of the G-tetrad, enhancing π–π interactions.[6] These molecules usually carry a positive charge to increase electrostatic interactions with the negatively charged DNA.[6] One challenge in the design of G-quadruplex binding ligands is obtaining selectivity for quadruplex over duplex DNA. In recent years, this has been accomplished with several small organic molecules,[7] with binding affinities typically at least ten-times greater for G-quadruplex DNA when compared to duplex DNA. An elegant approach to sensing has been achieved using fluorogenic ligands, where they brightly fluoresce upon binding to G-quadruplex DNA, allowing for selective visualization of G-quadruplex structures.[8] An emerging area of research aims to combine DNA sequence and structure selectivity with agents that can be triggered with external stimuli.[9]

Luminescent ruthenium(II) polypyridyl complexes have been used to detect duplex DNA as well as different DNA sequences, such as DNA mismatches or abasic sites.[10] Several compounds have also been shown to exhibit selectivity for G-quadruplex structures.[11] These complexes are typically $[Ru(bpy)_2L]$ or $[Ru(phen)_2L]$, where L is a derivative of imidazophenanthroline, bpy = 2,2′-bipyridine, and phen = 1,10-phenanthroline.[11a–c,g–l] As with the organic systems, the compounds interact primarily through π-stacking, which both induces the formation of G-quadruplexes and stabilizes these structures. Ru^{II} complexes containing dipyridylphenazine (dppz = dipyrido-[3,2-*a*:2′,3′-*c*] phenazine; see Figure 1, compound **1**) and its derivatives are known biological sensors due to their photophysical "light switching" ability, as they are non-luminescent ("dark") in aqueous environments but become luminescent ("bright") when intercalated into a duplex DNA base stack.[11d,f,n] This phenomenon is attributed to the presence of two closely spaced triplet metal-to-ligand charge transfer (^{3}MLCT) excited states; the "dark" state, localized on the phenazine portion of dppz, and the "bright" state, localized on the bipyridine portion of dppz. Taking advantage of this feature, Ru^{II} dppz derivatives have been reported as in vivo imagining agents.[12] Previously, we engineered intramolecular strain into a Ru^{II} polypyridyl complex using the 3,6-dimethyldipyridylphenazine (dmdppz) ligand (Figure 1), thereby lowering the energy of the triplet metal-centered (^{3}MC) state, which is an antibonding state.[13] The perturbation of the excited state energies presumably allowed for thermal population of this dissociative state from a ^{3}MLCT state, and resulted in light-induced ligand loss. This new molecule, $[Ru(bpy)_2dmdppz]^{2+}$ (**2**), acted as a photochemi-

[a] *E. Wachter, D. Moyá, Dr. S. Parkin, Dr. E. C. Glazer*
Department of Chemistry, University of Kentucky
505 Rose Street, Lexington, KY 40506 (USA)
E-mail: ec.glazer@uky.edu

Supporting information for this article is available on the WWW under http://dx.doi.org/10.1002/chem.201503203.

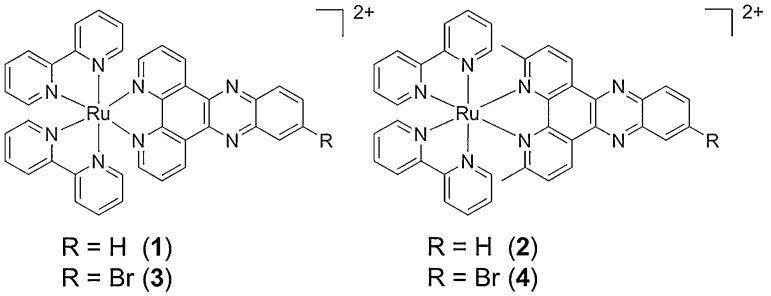

Figure 1. Structures of $[Ru(bpy)_2dppz]^{2+}$ (**1**), $[Ru(bpy)_2dmdppz]^{2+}$ (**2**) $[Ru(bpy)_2dppz\text{-}Br]^{2+}$ (**3**), and $[Ru(bpy)_2dmdppz\text{-}Br]^{2+}$ (**4**).

cal "light switch", and underwent rapid and selective ligand ejection in non-aqueous solvents and when bound to DNA.[14]

In our studies of $[Ru(bpy)_2dppz]^{2+}$ and $[Ru(bpy)_2dmdppz]^{2+}$, we observed enhanced emission intensity and photoreactivity in the K^+ folded telomeric G-quadruplex DNA over duplex DNA and proteins.[14] Generally, the photophysical properties of $[Ru(bpy)_2dppz]^{2+}$ paralleled the photochemical properties of $[Ru(bpy)_2dmdppz]^{2+}$.[15] Photochemical investigations of $[Ru(bpy)_2dmdppz]^{2+}$ supported a mechanism that was associative or interchange associative, with the chemical reaction potentially occurring from the ^{3}MLCT excited state.[15] This suggested that the binding environment of the complex could dictate its photochemical reactivity, which might allow for the development of structure-selective photochemical probes.

A recent crystal structure was reported describing a ruthenium polypyridyl complex with an asymmetric dppz ligand containing a substitution at the 11-position bound to duplex DNA. Λ-$[Ru(TAP)_2dppz\text{-}Cl]^{2+}$ (TAP = tetraazaphenanthrene) associates with duplex DNA through the dppz-Cl ligand intercalating in an angled binding mode, allowing for partial water occupancy near one phenazine nitrogen.[16] In contrast, the parent complex, Λ-$[Ru(TAP)_2dppz]^{2+}$, can intercalate more symmetrically, preventing any partial water occupancy.[16] As association between water molecules and one or more of the phenazine nitrogen atoms results in population of the "dark" state,[17] the interaction of a water molecule with the Cl-substituted ligand would be expected to result in reduced luminescence when the complex is bound to duplex DNA.[18] Given the binding orientation of the dppz-Cl ligand in duplex DNA, we hypothesized a similar substitution would induce a comparable binding mode. Additionally, we hypothesized that the increased surface area of G-quadruplex DNA would shield the substituted dppz ligand from occupancy of a water molecule near the phenazine nitrogen, allowing for enhanced selectivity for G-quadruplex over duplex DNA.

In this report, we describe two Ru^{II} polypyridyl complexes that contain a bromine at the 11-position of the intercalating dppz and dmdppz ligands, $[Ru(bpy)_2dppz\text{-}Br]^{2+}$ and $[Ru(bpy)_2dmdppz\text{-}Br]^{2+}$ (**3** and **4**; Figure 1). Complex **3** and **4** are derivatives of the photophysical "light switch" **1**, and our photochemical "light switch", **2**, respectively.[14,15,19] These molecules exhibit strong selectivity for G-quadruplex structures.

Results and Discussion

As seen in the crystal structures of **3** and **4** (Figure 2, and Figures S1 and S2, and Tables S3 and S4 in the Supporting Information), the addition of a bromo-substituent has little to no effect on the dppz-Br and dmdppz-Br ligands within the complex compared to their analogous parent ligands, dppz and dmdppz. The average Ru–N bond length deviates slightly on the dppz ligand (2.073 Å)[14] compared to the dppz-Br ligand (2.068 Å). Likewise, the average Ru–N bond length on the dmdppz ligand (2.104 Å)[14] is similar to the dmdppz-Br ligand (2.115 Å). The intramolecular strain in **4** is apparent from the 13° bend of the dmdppz-Br ligand out of plane, which is similar to the 15° bend seen for the dmdppz ligand.[14]

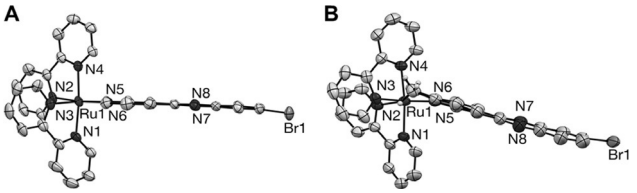

Figure 2. Ellipsoid plots of: A) **3**, and B) **4** showing the difference in distortion of the dppz-Br ligand and the dmdppz-Br ligand. Ellipsoids are drawn at 50% probability. The hydrogen atoms and minor disorder were omitted for clarity.

Interestingly, however, the bpy co-ligands in both complexes **3** and **4** experience increased distortion compared to the complexes **1** and **2** (Figure 3). This distortion is manifest through bending of the bpy out of plane as well as by twisting about the 2-2′ C–C bond. In **3**, the bpy co-ligands have an average bend and twist of 5.1° and 5.0°, respectively, which is approximately double the distortion seen for **1**.[14] Furthermore, the bpy co-ligands of **4** are bent by 6.7° and twisted by 4.0° on average, which is three times the distortion in **2**.[14] Comparing the orientation of the dppz/dmdppz ligands to the dppz-Br/dmdppz-Br ligands shows a drastic difference in the overall planarity of the ligand (Figure 3 and CIF files). The dppz-Br and the dmdppz-Br ligands are more planar than the dppz and dmdppz ligands, likely due to the lack of π-stacking interactions for **3** and **4** in the crystal lattice as a result of the addition of a bromo-substituent. The changes in distortion of **3** and **4** may play a role in imparting selectivity for binding and reacting with specific nucleic acid structures.

A high throughput screening (HTS) assay was developed to evaluate the interactions of the four complexes with 32 different biomolecules, including bovine serum albumin (BSA), nucleosides, duplex DNA, DNA sequences with mismatched bases, abasic sites, and bulges, as well as triplex DNA and G-quadruplex DNA. Conditions were optimized to minimize the

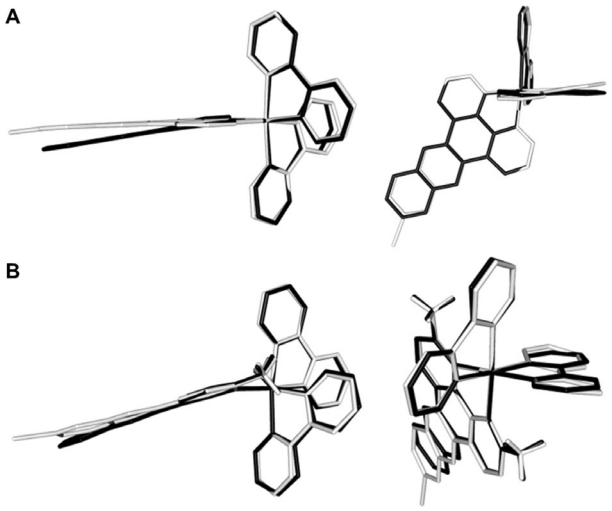

Figure 3. Overlays of the crystal structures of: A) **1** (black) and **3** (grey), and B) **2** (black) and **4** (grey) showing deviations in planarity of the dppz ligands (left) and the differences in the bpy co-ligands (right). Complexes **3** and **4** clearly exhibit increased distortion in the bpy co-ligands, and the overall orientation of the dppz ligands is quite different.

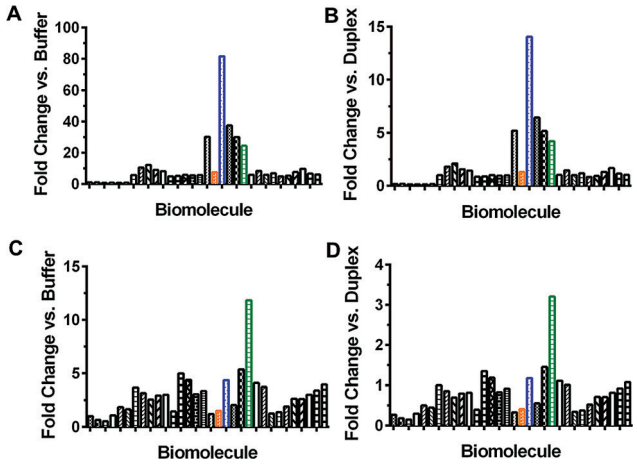

Figure 4. The luminescence fold change of **3** in different biomolecules in comparison to: A) buffer alone, and B) in CT DNA. The $t_{1/2}$ fold change of **4** in comparison to: C) buffer alone, and D) in CT DNA. Experimental conditions from left to right are in the order of Table S2 in the Supporting Information. Compound **3** is most selective for the intermolecular G-quadruplex (blue) and **4** is most selective for the telomeric G-quadruplex folded in the presence of K^+ ions (green). Neither compound shows a response when incubated with the telomeric G-quadruplex folded in the presence of Na^+ ions (orange).

amount of material used without compromising the data quality. Each ruthenium complex was screened under saturating DNA conditions (1:5 [Ru]/[DNA bp]) so that the complexes would be fully bound and could be compared independent of their binding affinities. The photophysical "light switch", **3**, was tested in triplicate in a 384-well plate, where luminescence was monitored by measuring full spectra. The photochemical "light switch", **4**, was tested under the same conditions, but in a 96-well format. The spectral changes associated with photochemical reactions were determined by measuring full absorbance spectra. For each experiment, compound **4** was irradiated with a 470 nm LED array for set times, and the absorbance was measured after each light exposure. The half-life ($t_{1/2}$) of ligand loss was then determined, and the presence of isosbestic points in the absorption spectra were used as an indication of a single photochemical reaction product. Both **3** and **4** exhibited enhanced behavior when incubated with the different DNA sequences when compared to buffer, and showed remarkable enhancement with G-quadruplex DNA over duplex DNA (Figure 4).

While compound **1** did not display a marked selectivity for any biomolecules (Figure S3 in the Supporting Information), when **3** was incubated with the different biomolecules, a significant preference for the intermolecular G-quadruplex was observed. This was manifest in an 82-fold luminescence enhancement over buffer alone (Figure 5, Table 1 and Table S5 in the Supporting Information). This selectivity for DNA secondary structure was also observed in a 14-fold increase in luminescence compared to CT DNA. Additionally, **3** was able to discriminate between different G-quadruplex sequences, as shown by the 2.7–11-fold increase in luminescence when bound to the intermolecular G-quadruplex compared to the other G-quadruplex sequences and structures (Table 1 and Table S5). Furthermore, **3** was also able to differentiate between the same telomeric G-rich sequence, [AGGG(TTAGGG)$_3$], under different conditions. When the DNA was folded in the presence of K^+ ions, the luminescence of **3** was three times greater than when the DNA was folded in the presence of Na^+ ions (Table 1 and Table S5).

The human telomeric sequence has been studied in the presence of Na^+ and K^+ ions and has been shown to form different structures depending on the cation, though some question remains as to the nature of these structures. When folded in the presence of Na^+, the G-quadruplex takes on an antiparallel basket structure.[20] In the presence of K^+ ions, however, the structure has been reported to be either parallel[21] or [3+1] mixed hybrid.[22] Multiple publications suggest that the structure of the telomeric sequence is dependent not only on the identity of the metal cations, but also DNA concentration and flanking nucleotide sequence.[23] Under our experimental conditions (see Experimental Section), we have tentatively assigned the telomeric sequence in the presence of K^+ ions as the mixed-hybrid structure, and as an antiparallel basket structure when folded with Na^+ ions.[24]

The photoreactivity of **4** was assessed when incubated with different biomolecules, and similar to the luminescent analogue **3**, it also exhibited a preference for G-quadruplexes. The complex was most reactive in the presence of the telomeric G-quadruplex folded in the presence of K^+ ions, with the rate of reaction increased twelve times over buffer alone and a 3.2× over CT DNA (Figure 4 and Figure 5, Table 1 and Table S5). Complex **4** showed a 1.5–5.4× increase in the rate of ligand ejection with the other G-quadruplex structures compared to buffer, making it 2–8× more sensitive to the K^+ G-quadruplex (Table 1 and Table S6 in the Supporting Information).

To determine if compounds **3** and **4** were selective for G-quadruplex structure, their sensing ability or reactivity was

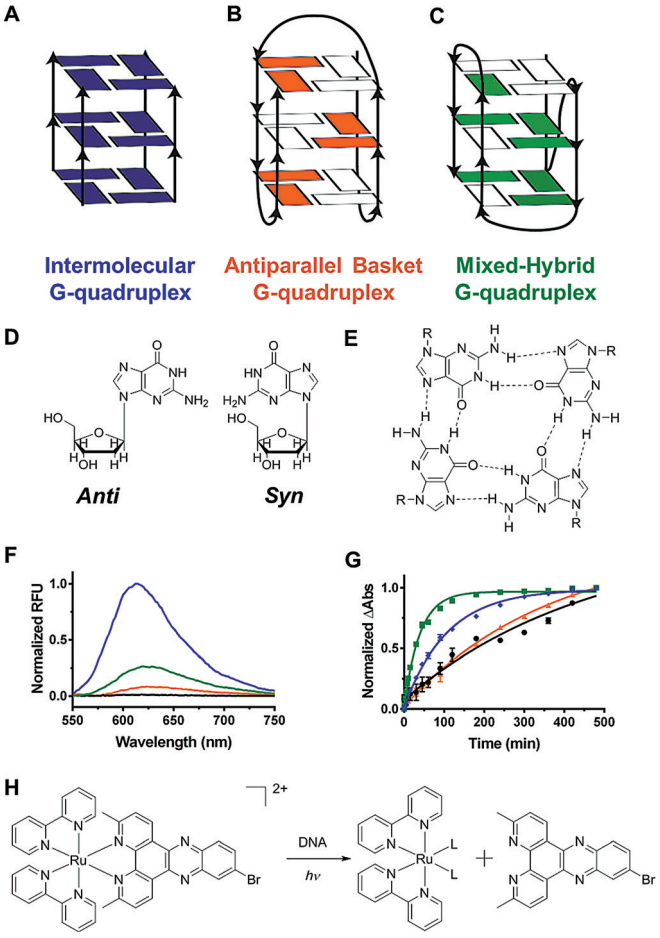

Figure 5. Selectivity of **3** and **4** for different G-quadruplex structures. A) Cartoon representation of the intermolecular G-quadruplex, B) telomeric (Na^+ folded) antiparallel basket G-quadruplex, and C) telomeric (K^+ folded) mixed-hybrid G-quadruplex, where colored boxes represent nucleotides in the *anti* conformation. D) The *anti* and *syn* orientation of guanosine. E) Hoogsteen base pairing of guanines in a G-quadruplex. F) Luminescence of **3** in buffer (black line), in the presence of the intermolecular G-quadruplex (blue line), the K^+ folded G-quadruplex (green line), and the Na^+ folded G-quadruplex (orange line) demonstrating increased sensitivity for the intermolecular G-quadruplex. G) Photoejection kinetics of **4** when irradiated in buffer (black line, ●), in the presence of the intermolecular G-quadruplex (blue line, ◆), the K^+ folded G-quadruplex (green line, ■), and the Na^+ folded G-quadruplex (orange line, ▲) showing the fastest reactivity with the K^+ folded G-quadruplex. H) Ligand loss reaction scheme for **4** when irradiated in the presence of DNA.

tested with duplex DNA with similar G content. A polyG·polyC duplex and a polyGC duplex were evaluated, and both complexes showed minimal activity with the sequences. Complex **3** had a 5.2–12.3× luminescence enhancement with various duplex sequences compared to buffer, while **4** was 1.5–3.7× more reactive with duplex DNA compared to buffer. Remarkably, these compounds are very selective for nucleic acids, as there was no enhancement in emission or reactivity for **3** and **4** with the hydrophobic protein BSA and neither complex was active with the nucleosides alone. Thus, the three-dimensional arrangement of the nucleic acids appears to mediate the selective photophysical and photochemical behavior of the complexes, as neither the individual components of a nucleic acid nor a hydrophobic protein elicit a response.

The sensitivity of **3** and **4** is pronounced compared to their parent complexes, **1** and **2**. When **2** was investigated for reactivity toward varying G-quadruplex structures, the complex was not able to discriminate between changes in folding or overall sequence, having only a 1–2× difference between G-quadruplex structures (Table S8 and Figure S3 in the Supporting Information). Additionally, the enhancement when compared to CT DNA was only at most a 4.4× increase. Similarly, **1** only exhibited an average of 2.6-fold improvement compared to other G-quadruplex structures and with a maximum of 1.4× increase over CT DNA (Table S7 and Figure S3 in the Supporting Information).

To discern what the major contributing factor for the sensitivity of **3** and **4** is, binding constants were determined with CT DNA, the mixed-hybrid G-quadruplex and the intermolecular G-quadruplex (Table S10 and Figures S9–S12 in the Supporting Information). Complex **3** had the highest binding affinity for the intermolecular G-quadruplex ($1.9\times10^6\,M^{-1}$), where as complex **4** had a greater binding affinity for the K^+ G-quadruplex ($6.1\times10^5\,M^{-1}$). The binding affinities paralleled the photophysical response of **3** and photochemical reactivity of **4**. In addition, the binding stoichiometries were determined for **1**–**4** using the Job plot continuous variation method (Table S10 and Figure S8 in the Supporting Information).[25] The complexes showed higher binding stoichiometries for G-quadruplex DNA over duplex DNA. Complexes **1**–**4** had >1:1 ratios of Ru/DNA when bound to the mixed-hybrid and intermolecular G-quadruplexes as evident by inflection points at $\chi > 0.5$. This unusual binding stoichiometry has been hypothesized to be caused by ruthenium complexes stacking on the DNA surface but does not give information on the binding mode of the complex to DNA.[25a] Along with high binding stoichiometries, **2** and **4** had broad Job plots, which may suggest multiple binding events or modes are occurring. Given the unusual binding stoichiometries of **3** and **4** to the intermolecular and mixed-hybrid G-quadruplex, respectively, it appears that the sensitivity of these complexes may be also influenced by the binding orientation within different DNA sequences and structures.

Table 1. Photophysical and photochemical properties of **3** and **4** with different G-quadruplex structures.

Condition[a]	Area **3**	Ratio to buffer **3**[b]	Ratio to duplex **3**[c]	$t_{1/2}$ [min] **4**	Ratio to buffer **4**[b]	Ratio to duplex **4**[c]
buffer	81 ± 10	1.0	0.2	330 ± 80[d]	1.0	0.3
inter	6600 ± 100	81.5	14.1	74 ± 8	4.5	1.2
c-myc	2440 ± 50	30.1	5.2	60 ± 4	5.5	1.5
Na^+[e]	620 ± 10	7.7	1.3	215 ± 3	1.5	0.4
K^+[e]	1990 ± 70	24.6	4.2	27 ± 2	12.2	3.2

[a] For full experimental details see the Experimental Section and Table S2 in the Supporting Information. [b] The luminescence area or $t_{1/2}$ fold change compared to buffer only. [c] The luminescence area or $t_{1/2}$ fold change compared to CT DNA. [d] Estimated $t_{1/2}$ for photodecomposition rather than photoejection of the dmdppz-Br ligand; the reaction was not complete after 8 h of light exposure. [e] Human telomeric sequence folded in the presence of the indicated cation.

In order to further probe the role the nucleic acid secondary structure played in the binding behavior of the complexes, circular dichroism (CD) was used to understand the interaction of **3** and **4** with the telomeric mixed-hybrid G-quadruplex and intermolecular G-quadruplex. The intermolecular G-quadruplex has four identical strands (5′-TAGGGTTA-3′) bound in a parallel orientation, and is characterized by a positive ellipticity at 260 nm (Figure S4 in the Supporting Information).[23b] Alternatively, the telomeric mixed-hybrid G-quadruplex is folded as an intramolecular G-quadruplex with three antiparallel strands and one parallel strand, as evident from the broad positive ellipticity at 290 nm (Figure S4).[23b,26]

Thermal CD melting points (T_m) for both G-quadruplexes were determined in the absence of compound, following incubation with each compound in the dark, and with **2** and **4** after irradiation (Figure 6 and Table S9 in the Supporting Information). Surprising differences were observed when the strained compounds **2** and **4** were incubated with the telomeric mixed-hybrid G-quadruplex in the dark compared to the unstrained molecules, **1** and **3**.

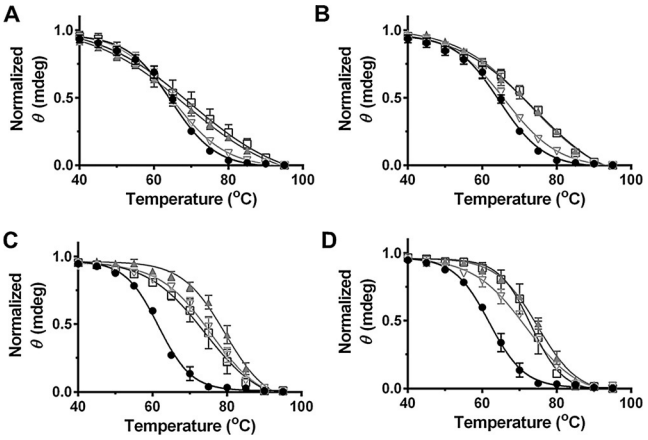

Figure 6. CD melting curves for: A) the mixed-hybrid G-quadruplex DNA only (●), with **3** (□), **4** in the dark (▲), and **4** following irradiation (▽). B) Mixed-hybrid G-quadruplex DNA only (●), with **1** (□), **2** in the dark (▲), and **2** following irradiation (▽). C) Intermolecular G-quadruplex DNA only (●), with **3** (□), **4** in the dark (▲), and **4** following irradiation (▽). D) Intermolecular G-quadruplex DNA only (●), with **1** (□), **2** in the dark (▲), and **2** following irradiation (▽).

Both strained molecules appeared to induce the formation of an intermediate DNA structure as the quadruplex melted, with greatest formation observed between 60 and 65 °C (Figure 7). This intermediate structure is characterized by a decrease in the positive ellipticity at 295 nm and an increase in the positive ellipticity at 260 nm. It has been proposed that this reflects the formation of a stable G-triplex intermediated in the melting process, with maximal signal at approximately 65 °C.[27] Based on our results, we hypothesize that the Ru^{II} complexes **2** and **4** are only interacting with and stabilizing one side of the mixed-hybrid structure, allowing for partial unfolding from the strand reversal loop side to form a G-triplex structure, as shown in Figure 7. This theory is further supported by analysis of the different G-quadruplex structures.

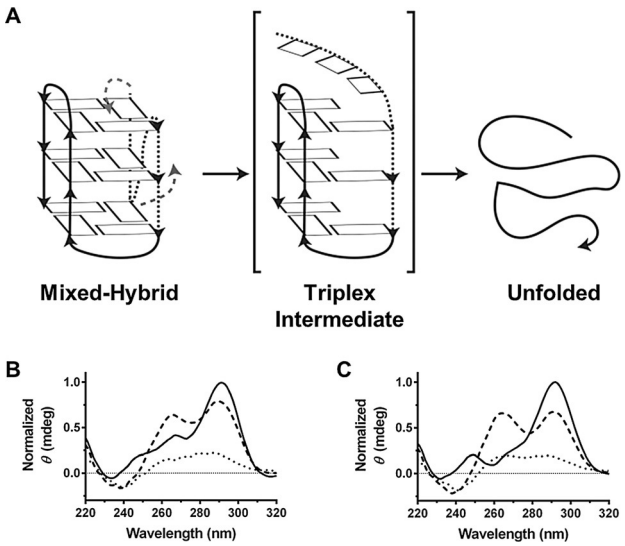

Figure 7. In the absence of irradiation, compounds **2** and **4** induce the formation of a semi-stable intermediate G-triplex at approximately 65 °C during thermal melting, as visualized by circular dichroism. A) Cartoon representation of the proposed unfolding pathway for the mixed-hybrid G-quadruplex. B) The CD spectra of **2**, and C) **4** at 25 °C (representing the mixed-hybrid, solid line); at 65 °C (representing the triplex intermediate formed, -----); and at 95 °C (representing the fully unfolded strand, ••••• line).

In general, all four Ru^{II} compounds have a stabilizing effect on both G-quadruplex structures, except when **2** and **4** are irradiated in the presence of the telomeric mixed-hybrid G-quadruplex. This difference would be consistent with a distinct binding mode of the strained complexes with this G-quadruplex compared to the intermolecular G-quadruplex. In the telomeric mixed-hybrid G-quadruplex, the guanosines are oriented with alternating *syn* and *anti* configurations as well as a strand reversal loop resulting in increased molecular crowding of the phosphate backbone that may inhibit intercalation (Figure 5 and Figure 8).[26] Therefore, the Ru^{II} complex may only bind as an end-capping molecule on either lateral loop faces, similar to other reports of Ru^{II} polypyridyl complexes with duplex and G-quadruplex DNA.[10b,26,30] In this type of binding mode, the dmdppz or dmdppz-Br ligand would only interact with one set of guanosines, rather than two sets in an intercalating binding mode, and facilitate the melting process through a triplex.

One question that was raised by this hypothesis of an end capping binding mode was the effect of the environment on the photochemistry of the complexes. Neither of the two molecules undergo photoejection in an aqueous environment, suggesting that the photochemical "light switch" effect relates to exposure of the phenazine nitrogen atoms to hydrogen bonding solvents, just as the photochemical "light switch" effect is controlled by exposure of these groups to water. However, when irradiated, both the dmdppz or dmdppz-Br ligands are photoejected from the Ru^{II} complex, allowing the Ru^{II} to metalate the DNA (Figures S5 and S6 in the Supporting Information).[14] This would require a binding mode where the dmdppz or dmdppz-Br ligands are shielded from the aqueous environment by the bases in the lateral loop(s), thereby allowing photoejection to occur. Upon the photoreaction, though,

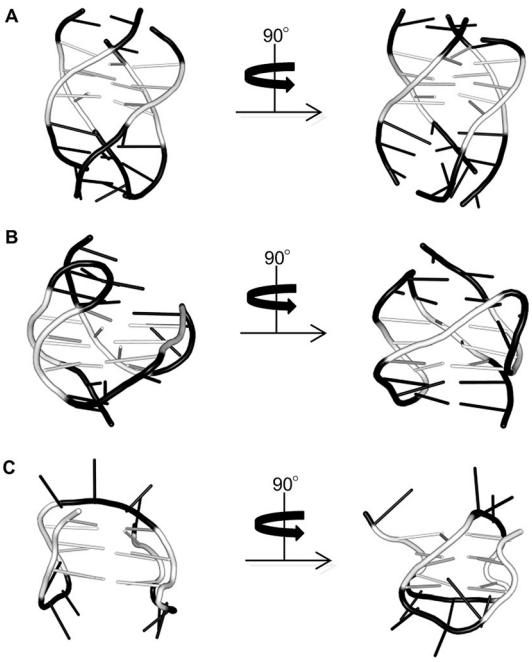

Figure 8. Orientation of the guanosine bases in: A) the intermolecular parallel G-quadruplex (PDB ID: 1NZM),[28] B) telomeric mixed-hybrid G-quadruplex (PDB ID: 2HY9),[29] and C) telomeric antiparallel basket G-quadruplex (PDB ID: 2 MCC).[26] The guanosines are shown in grey.

these end-capping dmdppz ligands could freely dissociate and would no longer provide a stabilizing effect for the G-quadruplex; therefore the T_m is comparable to DNA in the absence of complex. An alternative argument would be that when Ru^{II} metalation occurs it results in a destabilizing effect, which balances the stabilization induced by the dmdppz ligand, with the end result of a T_m comparable to DNA only.

The intramolecular antiparallel basket G-quadruplex also experiences irregular spacing of the phosphate backbone (Figure 8), and the Ru^{II} complexes will likely bind through an end-capping mechanism. However, when **1**–**4** are incubated with the Na^+ folded telomeric sequence they show diminished activity compared to the K^+ structure. If the complexes bind through a similar end-capping mechanism through the diagonal or lateral loops of the antiparallel basket structure, the loops must not be shielding the phenazine nitrogen atoms to the same extent as in the mixed-hybrid structure. This may be due to the loop bases being flipped out in the antiparallel basket structure and unable to shield the phenazine nitrogen atoms properly. If these Ru^{II} complexes are binding through an end-capping mechanism, the loop regions seem to be important for determining the activity of these molecules.

In the intermolecular G-quadruplex, in contrast, all of the guanosines are in an *anti* configuration, resulting in a regular molecular spacing of the phosphate backbone (Figure 8), allowing for potential intercalation of the dmdppz or dmdppz-Br ligand.[21] Additionally, there are no loops in the intermolecular G-quadruplex which allows for stacking of an intercalating ligand between two individual G-quadruplexes. Independent of which binding mode occurs, **2** and **4** stabilize the intermolecular G-quadruplex, likely through π-stacking interactions with the dmdppz or dmdppz-Br ligand, as demonstrated by the 13–18° shift in the T_m. When irradiated with light, the stabilization of the G-quadruplex is maintained and metalation of the DNA occurs (Figure S6 in the Supporting Information). This suggests that a stronger, longer lived stabilizing interaction is taking place in the intermolecular structure. Based on the fact that the T_m remains unchanged upon irradiation, we predict that either the dmdppz or dmdppz-Br ligand is unable to dissociate from its intercalated position following DNA metalation, or alternatively, the metalation stabilizes the structure.

Interestingly, **3** induces a structural change when bound to the mixed-hybrid G-quadruplex that we hypothesize is either from a change in folding or through ion displacement upon Ru^{II} binding. This change is visualized by an increased positive ellipticity at 250 nm while maintaining a positive ellipticity at 295 nm. This spectral shift and degree of stabilization is not seen for its parent complex **1** (Figure S7 in the Supporting Information). This may provide additional evidence that the substitution at the 11-position is a key feature in directing activity of these molecules to specific DNA sequences and structures.

Conclusion

Complexes **3** and **4** are "light switches" that show significant selectivity towards the parallel intermolecular G-quadruplex and telomeric mixed-hybrid G-quadruplex, respectively. Subtle changes in the structures of the complexes, caused by intramolecular strain, resulted in dissimilar interactions with the G-quadruplexes. These changes have an affect on the binding affinity, and we hypothesize that they induce differences in the binding modes for the two G-quadruplex structures that result in photophysical and photochemical selectivity. Complex **3** has a planar dppz-Br ligand that is more likely to interact through intercalative binding, whereas distortion of complex **4** may lead to the nonplanar dmdppz-Br ligand interacting through end-capping at the lateral loop end. Since the phosphate backbone of the intermolecular G-quadruplex is equally spaced and lacks loops, the planar dppz ligand of **3** can intercalate more easily within the G-quadruplex or between two G-quadruplexes, compared to the crowded backbone and loop containing telomeric mixed-hybrid G-quadruplex. This could result in the heightened selectivity for the intermolecular G-quadruplex. Compound **4**, in contrast, with a distorted planar dppz ligand, would interact more favorably in an end-capping binding mode where the loop regions shield the phenazine nitrogen atoms, and the compound exhibits greater selectivity for the telomeric mixed-hybrid G-quadruplex. These differences give rise to two complexes with different modes of activation, and may prove to be useful for rational design of G-quadruplex targeting molecules for in vivo applications.[12a,b]

Experimental Section

Materials and instrumentation

All chemicals were of reagent grade and were used without further purification. *cis*-Dichlorobis(2,2′-bipyridine)ruthenium(II) dihydrate

was purchased from Strem Chemicals and 4-bromo-*o*-phenylenediamine was purchased from AlfaAesar. Custom DNA sequences were purchased from Eurofins. All ^{1}H NMR and ^{13}C NMR spectra were obtained on a Varian Mercury spectrometer (400, 100 MHz). The ^{1}H chemical shifts are reported relative to the residual solvent peak of CD_3CN at $\delta = 1.94$ ppm. The ^{13}C chemical shifts are referenced to CD_3CN at $\delta = 1.39$ ppm. Electrospray ionization (ESI) mass spectra were obtained on a Varian 1200 L mass spectrometer at the Environmental Research Training Laboratory (ERTL) at the University of Kentucky. UV/Vis absorption spectra were obtained on a BMG Labtech FLUOstar Omega microplate reader. Light activation for photoejection experiments was achieved using a 470 nm LED array from Elixa. Luminescence spectra were obtained on a Molecular Devices Spectramax M5 microplate reader. CD experiments were performed on a Jasco J-815 CD Spectrometer equipped with a MPTC-490S/15 temperature controller. HPLC experiments were run on an Agilent 1100 Series HPLC equipped with a model G1311A quaternary pump, G1315B UV diode array detector and Chemstation software version B.01.03. Chromatographic conditions were optimized on a Column Technologies Inc. C18 120 Å column (for purity analysis) and a Grace Davison Discovery Science (Vydac 218TP C18 5 μm) C18 column (for adduct formation analysis) fitted with a Phenomenex C18 guard column. The Prism software package was used to analyze kinetic data with a single exponential equation, luminescence spectra with area under the curve, and melting temperature using a sigmoidal dose response equation.

Synthesis and characterization

1,10-Phenanthroline-5,6-dione (phendione) was prepared as previously reported.[31] 2,9-Dimethyl-1,10-phenanthroline-5,6-dione (dmphendione) was prepared in an analogous manner as phendione using 2,9-dimethyl-1,10-phenanthroline. The synthesis of $[Ru(bpy)_2dppz]^{2+}$ (**1**) and $[Ru(bpy)_2dmdppz]^{2+}$ (**2**) was previously reported.[14] Note: the numbering for phen and dppz ligands is different. The 2,9 positions on phen are *ortho* to the pyridyl nitrogen atoms, analogues to the 3,6 positions on dppz.

11-Bromo-3,6-dimethyldipyrido[3,2-*a*:2′,3′-*c*]phenazine (dmdppz-Br): The compound was prepared by slight modification to a previously reported procedure.[32] 2,9-Dimethyl-1,10-phenanthroline-5,6-dione (100 mg, 0.420 mmol) and 4-bromo-*o*-phenylenediamine (88 mg, 0.471 mmol) were suspended in ethanol (4 mL) and refluxed at 80 °C for 4 h. The resulting brown suspension was filtered and washed with cold ethanol. The product was collected in 48% yield (79 mg) as a brown solid and used without further purification.

$[Ru(bpy)_2phendione](PF_6)_2$:[33] $[Ru(bpy)_2Cl_2]\cdot 2H_2O$ (100 mg, 0.192 mmol) and 1,10-phenanthroline-5,6-dione (55 mg, 0.262 mmol) were dissolved in ethanol (20 mL) and refluxed at 80 °C for 2 h. The resulting yellow-brown mixture was cooled to room temperature and precipitated with 3 mL of a saturated aqueous KPF_6 solution. The precipitate was filtered and washed with water and ether. The product was obtained in 85% yield (150 mg) as a brown solid. ^{1}H NMR (CD_3CN, 400 MHz): $\delta = 8.54$–8.50 (m, 6H), 8.09 (tt, $J = 7.8$, 1.2 Hz, 4H), 7.94 (dd, $J = 5.5$, 1.2 Hz, 2H), 7.85–7.84 (m, 2H), 7.76–7.74 (m, 2H), 7.61 (2d, $J = 7.8$, 8.2 Hz, 2H), 7.45–7.41 ppm (m, 4H); ESI MS $C_{32}H_{22}N_6O_2Ru$: *m/z* calcd $[M]^+$ PF_6^- 769.08, $[M]^{2+}$ 312.04, found 768.70 $[M]^+$ PF_6^-, 312.10 $[M]^{2+}$.

$[Ru(bpy)_2dppz\text{-}Br](PF_6)_2$ (3):[32] This complex was synthesized following a procedure reported for similar compounds.[33] A solution of $[Ru(bpy)_2phendione](PF_6)_2$ (68 mg, 0.074 mmol) and 4-bromo-*o*-phenylenediamine (18 mg, 0.096 mmol) in ethanol (8 mL) was refluxed at 80 °C for 1 h. The resulting red mixture was cooled to room temperature, diluted with water, filtered and washed with water and ether. Purification by flash chromatography (silica, eluting at 80:20:0.1 acetonitrile/water/saturated KNO_3) gave the pure product. The solvent was removed under vacuum, and the complex was converted to PF_6^- salt. The product was obtained in 96% yield (76 mg) as a crystalline red solid. ^{1}H NMR (CD_3CN, 400 MHz): $\delta = 9.62$ (ddd, $J = 8.2$, 7.6, 1.2 Hz, 2H), 8.70 (d, $J = 2.7$ Hz, 1H), 8.55 (d, $J = 8.2$ Hz, 2H), 8.52 (d, $J = 8.21$ Hz, 2H), 8.37 (d, $J = 9.0$ Hz, 1H), 8.21 (dd, $J = 9.0$, 2.0 Hz, 1H), 8.18 (dt, $J = 5.5$, 1.6 Hz, 2H), 8.12 (td, $J = 8.0$, 7.8, 1.6 Hz, 2H), 8.02 (td, $J = 8.0$, 7.8, 1.6 Hz, 2H), 7.89 (ddd, $J = 8.2$, 5.5, 2.7 Hz, 2H), 7.86–7.84 (m, 2H), 7.73–7.72 (m, 2H), 7.47 (ddd, $J = 7.5$, 5.5, 1.2 Hz, 2H), 7.26 ppm (ddd, $J = 7.5$, 5.9, 1.2 Hz, 2H); ^{13}C NMR (CD_3CN, 100 MHz): $\delta = 158.28$, 158.08, 155.12, 155.01, 153.23, 153.07, 151.81, 151.64, 144.12, 142.63, 141.77, 141.40, 139.10, 139.02, 136.83, 134.67, 134.60, 132.73, 132.27, 131.73, 131.63, 128.73, 128.62, 128.58, 127.38, 125.44, 125.38 ppm; Purity by HPLC: 99.9% by area; UV/Vis in CH_3CN, λ_{max} (ε) = 285 (107400), 365 (21100), 443 nm (18700 $M^{-1}cm^{-1}$); ESI MS calcd for $C_{38}H_{25}BrN_8Ru$: $[M]^+$ PF_6^- 919, $[M]^{2+}$ 387.02, found 919.1 $[M]^+$ PF_6^-, 386.9 $[M]^{2+}$.

$[Ru(bpy)_2dmdppz\text{-}Br](PF_6)_2$ (4): A solution of $[Ru(bpy)_2Cl_2]\cdot 2H_2O$ (75 mg, 0.144 mmol) and dmdppz-Br (81 mg, 0.208 mmol) in ethylene glycol (8 mL) was stirred at 120 °C for 3 h. The resulting mixture was cooled and transferred to an Erlenmeyer flask with water. The aqueous product was precipitated upon the addition of a saturated aqueous KPF_6 solution, filtered and washed with water and ether. Purification by flash chromatography (silica, eluting at 85:15:0.1 acetonitrile/water/saturated KNO_3) gave the pure product. The solvent was removed under vacuum, and the complex was converted to PF_6^- salt. The product was obtained in 65% yield (102 mg) as a crystalline red solid. ^{1}H NMR (CD_3CN, 400 MHz): $\delta =$ 9.60 (t, $J = 8.2$ Hz, 2H), 8.66 (dd, $J = 2.2$, 0.5 Hz, 1H), 8.52–8.45 (m, 4H), 8.34 (dd, $J = 9.1$, 0.5 Hz, 1H), 8.18 (dd, $J = 9.1$, 2.2 Hz, 1H), 8.07–7.98 (m, 4H), 7.85–7.83 (m, 2H), 7.79 (dd, $J = 8.3$, 2.0 Hz, 2H), 7.71 (dq, $J = 6.3$, 0.7 Hz, 2H), 7.32–7.26 (m, 4H), 1.95 ppm (s, 6H); ^{13}C NMR (CD_3CN, 100 MHz): $\delta = 170.08$, 169.97, 158.64, 158.48, 154.18, 154.16, 152.97, 152.93, 152.77, 144.28, 142.78, 140.98, 140.65, 139.09, 138.89, 136.45, 135.36, 135.31, 132.57, 132.15, 129.74, 129.33, 129.23, 128.61, 128.49, 126.97, 125.66, 125.56, 26.54, 26.52 ppm; Purity by HPLC: 99.9% by area; UV/Vis in CH_3CN, λ_{max} (ε) = 285 (116300), 365 (23700), 443 nm (18500 $M^{-1}cm^{-1}$); ESI MS calcd for $C_{40}H_{29}BrN_8Ru$: $[M]^+$ PF_6^- 947.03, $[M]^{2+}$ 401.04, found 946.8 $[M]^+$ PF_6^-, 400.7 $[M]^{2+}$.

Counterion exchange

Compounds **1**–**4** were converted to Cl^- salts by dissolving 5–20 mg of product in 1–2 mL methanol. The dissolved product was loaded onto an Amberlite IRA-410 chloride ion exchange column, eluted with methanol, and the solvent was removed in vacuo.

HPLC analysis for purity

The purity of each Ru^{II} complex was analyzed using mobile phases of 0.1% formic acid in dH_2O and 0.1% formic acid in HPLC grade CH_3CN were used. Samples of each Ru^{II} complex were prepared in dH_2O and protected from light before injection on the HPLC. See Table S1 in the Supporting Information for the gradient used.

Luminescence and photoejection studies

Table S2 in the Supporting Information provides detailed information of the different protein, nucleoside and DNA sequences tested with compounds **1**–**4**. In brief, DNA sequences were resuspended

in buffer, incubated at room temperature for 15 min, vortexed, and annealed prior to testing. Following heating to the specified annealing temperature, the DNA was cooled slowly to room temperature then stored at 4 °C, overnight. Bovine serum albumin (BSA), deoxyadenosine (dA), deoxyguanosine (dG), thymidine (dT), and deoxycytosine (dC) were resuspended in buffer to give a 1 mM stock. Calf thymus DNA (CT DNA) was resuspended and sonicated as reported previously.[14] All biomolecules were stored long term at −20 °C.

Luminescence studies: The emission of **1** and **3** were tested at 5 μM in the presence of 25 μM of each biomolecule given in Table S2 in the Supporting Information in triplicate in a Greiner black/clear bottom 384-well plate. For DNA sequences the concentration is measured in [bp] and the ratio of [Ru]/[bp] was 1:5. A final volume of 25 μL was used for all samples. Data collection was performed with $\lambda_{ex}=440$ nm and $\lambda_{em}=550$–750 nm.

Photoejection studies: The kinetics for ligand ejection for **2** and **4** (20 μM; Cl^- counter-ions) given in Table S2 was determined in triplicate in a Greiner UV clear half-area 96-well plate. Samples were measured in the presence of 100 μM of each biomolecule, with a final volume of 50 μL. For DNA sequences the concentration is measured in [bp] and the ratio of [Ru]/[bp] was 1:5. The well plate was positioned 12 inches below a 470 nm LED array, and full spectra were collected after set time points of light exposure for a total of 8 h. The normalized change in absorbance was plotted versus time to give the $t_{1/2}$ of ligand loss.

Thermal DNA melts by circular dichroism

Compounds **1**–**4** were incubated with 25 μM K^+ folded telomeric G-quadruplex and 50 μM intermolecular G-quadruplex at a 2:1 [Ru]/[DNA bp] ratio in the dark. Samples of **2** and **4** were also irradiated with 470 nm light for 7 h in the presence of DNA. The DNA in the absence of compound was used as the control. All samples were incubated at room temperature, overnight. Following incubation, samples were melted from 25–95 °C taking measurements every 5 °C and the CD signal was monitored from 220–320 nm. The normalized change in ellipticity was plotted versus temperature to give the melting temperature (T_m). All samples were run in duplicate.

Adduct formation determined by HPLC

The K^+ folded telomeric G-quadruplex and intermolecular G-quadruplex (250 μM nucleotide concentration) were incubated with 500 μM **4** either in the dark or under irradiated with 470 nm light for 3 h. Samples were then incubated at 37 °C, overnight, before HPLC analysis. The DNA in the absence of compound was run as a reference.

DNA binding

Absorbance binding titrations of **1**–**4** were performed in a half-area 96-well plate with 20 μM Ru^{II} and a total volume of 150 μL. The absorbance was measured after each DNA addition from 0–4.5 equivalents of DNA (CT DNA, K^+ G-quadruplex or intermolecular G-quadruplex). Samples were allowed to equilibrate for 5 min prior to measuring the absorbance. The data were corrected for any dilution of the Ru^{II} complex during the titration. Binding constants were determined using Prism software.

Binding stoichiometries were determined for **1**–**4** with CT DNA, the K^+ G-quadruplex, and the intermolecular G-quadruplex using the method of continuous variation. Solutions of each complex and DNA were prepared at 1 mM in the appropriate buffer (Table S2). The total concentration was kept constant at 80 μM while the [Ru] and [DNA] were varied from 0–1 mol fraction Ru^{II} and 1–0 mol fraction DNA. Samples were prepared in a half area 96-wel plate with a total volume of 100 μL. The Ru^{II} only absorbance was measured prior to the addition of DNA. The absorbance was adjusted for any dilution due to DNA addition. Following DNA addition the samples were incubated for 15 min prior to measuring the absorbance. The change in absorbance was plotted versus mol fraction of Ru^{II} (χ_{Ru}) to generate a Job plot. Linear regression analysis was performed using Prism software.

Crystallography

Since the compounds are known to be unstable with respect to light, all crystal manipulations requiring light were conducted as rapidly as possible.

Single crystals of **3** were grown from acetone by vapor diffusion of diethyl ether, then mounted in inert oil and transferred to the cold gas stream of the diffractometer. X-ray diffraction data were collected at 90.0(2) K on a Bruker-Nonius X8 Proteum diffractometer with graded-multilayer focused $Cu_{K\alpha}$ X-rays. Raw data were integrated, scaled, merged and corrected for Lorentz-polarization effects using the APEX2 package.[34] Corrections for absorption were applied using either SADABS or TWINABS,[35] and by XABS2.[36] The structure was solved by direct methods (SHELXS-97)[36] and difference Fourier (SHELXL-97).[37] Refinement was carried out against F^2 by weighted full-matrix least-squares (SHELXL-97),[37] and assessed with the aid of an *R*-tensor.[38] Hydrogen atoms were found in difference maps but subsequently placed at calculated positions and refined using a riding model. Non-hydrogen atoms were refined with anisotropic displacement parameters. Atomic scattering factors were taken from the International Tables for Crystallography.[39] Crystal data and relevant details of the structure determinations are summarized below and selected geometrical parameters are given in Table S3 in the Supporting Information.

Crystal data (3): $C_{44}H_{36}BrF_{12}N_8O_2P_2Ru$, $M_r=1179.73$, triclinic, $P\bar{1}$, $a=9.3281(4)$ Å, $b=13.0620(6)$ Å, $c=19.8864(8)$ Å, $\alpha=96.696(2)^\circ$, $\beta=96.947(2)^\circ$, $\gamma=103.634(2)^\circ$, $V=2310.87$ Å^3, $Z=2$, $\rho=1.695$ mg m^{-13}, $\mu=5.280$ mm^{-1}, $\lambda=1.54178$ Å, $T=90.0(2)$ K, $F(000)=1178$, crystal size $=0.170\times0.100\times0.080$ mm, $\theta(\max)=68.208^\circ$, 29528 reflections collected, 8159 unique reflections ($R_{int}=0.0538$), GOF $=1.102$, $R_1=0.0667$ and $wR_2=0.1540$ [$I>2\sigma(I)$], $R_1=0.0686$ and $wR_2=0.1552$ (all indices), largest difference peak/hole $=1.265/-1.341$ e Å^{-3}.

Single crystals of **4** were crystallized from methylene chloride by vapor diffusion of tetrahydrofuran, mounted in inert oil and transferred to the cold gas stream of the diffractometer. X-ray diffraction data were collected at 90.0(2) K on a Nonius κCCD diffractometer using $Mo_{K\alpha}$ X-rays. Raw data were integrated, scaled, merged and corrected for Lorentz-polarization effects using the HKL-SMN package.[40] Corrections for absorption were applied using either SCALEPACK,[40] or SADABS,[35] and by XABS2.[36] The structure was solved by direct methods (SHELXS-97)[37] and difference Fourier (SHELXL-97).[37] Refinement was carried out against F^2 by weighted full-matrix least-squares (SHELXL-97),[37] with the aid of an *R*-tensor.[38] Hydrogen atoms were found in difference maps but subsequently placed at calculated positions and refined using a riding model. Non-hydrogen atoms were refined with anisotropic displacement parameters. Atomic scattering factors were taken from the International Tables for Crystallography.[39] Crystal data and relevant details of the structure determinations are summarized below and selected geometrical parameters are given in Table S4 in the Supporting Information.

Crystal data (4): $C_{40}H_{29}BrF_{12}N_8O_2P_2Ru$, $M_r = 1092.63$, monoclinic, $P2_1/c$, $a = 10.7998(5)$ Å, $b = 12.6135(6)$ Å, $c = 34.0173(15)$ Å, $\alpha = 90^\circ$, $\beta = 96.2404(11)^\circ$, $\gamma = 90^\circ$, $V = 4606.4(4)$ Å^3, $Z = 4$, $\rho = 1.575$ mg m^{-13}, $\mu = 1.364$ mm^{-1}, $\lambda = 0.71073$ Å, $T = 90.0(2)$ K, $F(000) = 2168$, crystal size $= 0.240 \times 0.210 \times 0.180$ mm, $\theta(\max) = 27.559^\circ$, 74251 reflections collected, 10589 unique reflections ($R_{int} = 0.0494$), GOF = 1.080, $R_1 = 0.0478$ and $wR_2 = 0.1261$ [$I > 2\sigma(I)$], $R_1 = 0.0776$ and $wR_2 = 0.1499$ (all indices), largest difference peak/hole = 0.874/−0.820 e Å^{-3}.

CCDC 1416015 (**3**) and 1416014 (**4**) contain the supplementary crystallographic data for this paper. These data can be obtained free of charge from The Cambridge Crystallographic Data Centre.

Acknowledgements

This work was supported by the American Cancer Society (RSG-13-079-01-CDD) and the National Institutes of Health (R01M107586). E.W. was supported by the University of Kentucky Research Challenge Trust Fund Fellowship. We would also like to thank the University of Kentucky Environmental Research Training Laboratory (ERTL) for assisting with chemical analysis. The luminescence plate reader experiments were performed on an Instrument in the Center for Molecular Medicine Protein Core, which is funded through NIH/NIGMS COBRE grant P30M110787.

Keywords: G-quadruplexes · light switch · photochemistry · photophysics · ruthenium

[1] a) S. Burge, G. N. Parkinson, P. Hazel, A. K. Todd, S. Neidle, *Nucleic Acids Res.* **2006**, *34*, 5402 – 5415; b) S. Balasubramanian, S. Neidle, *Curr. Opin. Chem. Biol.* **2009**, *13*, 345 – 353; c) T.-M. Ou, Y.-J. Lu, J.-H. Tan, Z.-S. Huang, K.-Y. Wong, L.-Q. Gu, *ChemMedChem* **2008**, *3*, 690 – 713.

[2] a) R. I. Mathad, E. Hatzakis, J. Dai, D. Yang, *Nucleic Acids Res.* **2011**, *39*, 9023 – 9033; b) A. Siddiqui-Jain, C. L. Grand, D. J. Bearss, L. H. Hurley, *Proc. Natl. Acad. Sci. USA* **2002**, *99*, 11593 – 11598.

[3] S. Rankin, A. P. Reszka, J. Huppert, M. Zloh, G. N. Parkinson, A. K. Todd, S. Ladame, S. Balasubramanian, S. Neidle, *J. Am. Chem. Soc.* **2005**, *127*, 10584 – 10589.

[4] T. S. Dexheimer, D. Sun, L. H. Hurley, *J. Am. Chem. Soc.* **2006**, *128*, 5404 – 5415.

[5] S. Neidle, G. Parkinson, *Nat. Rev. Drug Discovery* **2002**, *1*, 383 – 393.

[6] a) J. L. Huppert, *Chem. Soc. Rev.* **2008**, *37*, 1375 – 1384; b) D. Monchaud, M.-P. Teulade-Fichou, *Org. Biomol. Chem.* **2008**, *6*, 627 – 636.

[7] a) N. W. Luedtke, *Chimia* **2009**, *63*, 134 – 139; b) R. Rodriguez, S. Müller, J. A. Yeoman, C. Trentesaux, J.-F. Riou, S. Balasubramanian, *J. Am. Chem. Soc.* **2008**, *130*, 15758 – 15759; c) A. De Cian, E. DeLemos, J.-L. Mergny, M.-P. Teulade-Fichou, D. Monchaud, *J. Am. Chem. Soc.* **2007**, *129*, 1856 – 1857; d) S. Sparapani, S. M. Haider, F. Doria, M. Gunaratnam, S. Neidle, *J. Am. Chem. Soc.* **2010**, *132*, 12263 – 12272; e) M. Bejugam, M. Gunaratnam, S. Müller, D. A. Sanders, S. Sewitz, J. A. Fletcher, S. Neidle, S. Balasubramanian, *ACS Med. Chem. Lett.* **2010**, *1*, 306 – 310.

[8] a) A. C. Bhasikuttan, J. Mohanty, *Chem. Commun.* **2015**, *51*, 7581 – 7597; b) A. Renaud de La Faverie, A. Guédin, A. Bedrat, L. A. Yatsunyk, J.-L. Mergny, *Nucleic Acids Res.* **2014**, *42*, e65; c) F. Koeppel, J.-F. Riou, A. Laoui, P. Mailliet, P. B. Arimondo, D. Labit, O. Petitgenet, C. Hélène, J.-L. Mergny, *Nucleic Acids Res.* **2001**, *29*, 1087 – 1096; d) M. Tera, K. Iida, K. Ikebukuro, H. Seimiya, K. Shin-ya, K. Nagasawa, *Org. Biomol. Chem.* **2010**, *8*, 2749 – 2755; e) B. Jin, X. Zhang, W. Zheng, X. Liu, C. Qi, F. Wang, D. Shangguan, *Anal. Chem.* **2014**, *86*, 943 – 952; f) L. Zhang, J. C. Er, X. Li, J. J. Heng, A. Samanta, Y.-T. Chang, C.-L. Lee, *Chem. Commun.* **2015**, *51*, 7386 – 7389.

[9] M. Nadai, F. Doria, L. Germani, S. N. Richter, M. Freccero, *Chem. Eur. J.* **2015**, *21*, 2330 – 2334.

[10] a) M. H. Lim, H. Song, E. D. Olmon, E. E. Dervan, J. K. Barton, *Inorg. Chem.* **2009**, *48*, 5392 – 5497; b) H. Song, J. T. Kaiser, J. K. Barton, *Nat. Chem.* **2012**, *4*, 615 – 620; c) A. J. McConnell, M. H. Lim, E. D. Olmon, H. Song, E. E. Dervan, J. K. Barton, *Inorg. Chem.* **2012**, *51*, 12511 – 12520; d) C. M. Shade, R. D. Kennedy, J. L. Rouge, M. S. Rosen, M. X. Wang, S. E. Seo, D. J. Clingerman, C. A. Mirkin, *Chem. Eur. J.* **2015**, *21*, 10983 – 10987.

[11] a) J. Zhang, Q. Yu, Q. Li, L. Yang, L. Chen, Y. Zhou, J. Liu, *J. Inorg. Biochem.* **2014**, *134*, 1 – 11; b) G. Liao, X. Chen, J. Wu, C. Qian, H. Wang, L. Ji, H. Chao, *Dalton Trans.* **2014**, *43*, 7811 – 7819; c) Q. Li, J. Zhang, L. Yang, Q. Yu, Q. Chen, X. Qin, F. Le, Q. Zhang, J. Liu, *J. Inorg. Biochem.* **2014**, *130*, 122 – 129; d) J.-L. Yao, X. Gao, W. Sun, S. Shi, T.-M. Yao, *Dalton Trans.* **2013**, *42*, 5661 – 5672; e) J. Wang, Y. Chen, J. Ren, C. Zhao, X. Qu, *Nucleic Acids Res.* **2014**, *42*, 3792 – 3802; f) X.-H. Lu, S. Shi, J.-L. Yao, X. Gao, H.-L. Huang, T.-M. Yao, *J. Inorg. Biochem.* **2014**, *140*, 64 – 71; g) D. Sun, Y. Liu, Q. Yu, D. Liu, Y. Zhou, J. Liu, *J. Inorg. Biochem.* **2015**, DOI: 10.1016/j.jinorgbio.2015.04.003; h) Z. Zhang, Q. Wu, X.-H. Wu, F.-Y. Sun, L.-M. Chen, J.-C. Chen, S.-L. Yang, W.-J. Mei, *Eur. J. Med. Chem.* **2014**, *80*, 316 – 324; i) G. Liao, X. Chen, J. Wu, C. Qian, Y. Wang, L. Ji, H. Chao, *Dalton Trans.* **2015**, *44*, 15145 – 15156; j) Z. Zhang, X.-H. Wu, F.-Q. Sun, F. Shan, J.-C. Chen, L.-M. Chen, Y.-S. Zhou, W.-J. Mei, *Inorg. Chim. Acta* **2014**, *418*, 23 – 29; k) Q. Yu, Y. Liu, J. Zhang, F. Yang, D. Sun, D. Liu, Y. Zhou, J. Liu, *Metallomics* **2013**, *5*, 222 – 231; l) Y. Xia, Q. Chen, X. Y. Qin, D. Sun, J. Zhang, J. Liu, *New J. Chem.* **2013**, *37*, 3706 – 3715; m) S. Shi, J.-H. Xu, X. Gao, H.-L. Huang, T.-M. Yao, *Chem. Eur. J.* **2015**, *21*, 11435 – 11445; n) S. Shi, X. Geng, J. Zhao, T. Yao, C. Wang, D. Yang, L. Zheng, L. Ji, *Biochimie* **2010**, *92*, 370 – 377.

[12] a) M. Matson, F. R. Svensson, B. Nordén, P. Lincoln, *J. Phys. Chem. B* **2011**, *115*, 1706 – 1711; b) F. R. Svensson, M. Abrahamsson, N. Strömberg, A. G. Ewing, P. Lincoln, *J. Phys. Chem. Lett.* **2011**, *2*, 397 – 401; c) Other reports, however, demonstrate that some $[Ru(L)_2dppz]$ complexes are cytotoxic.

[13] a) J. Van Houten, R. J. Watts, *Inorg. Chem.* **1978**, *17*, 3381 – 3385; b) B. Durham, J. V. Caspar, J. K. Nagle, T. J. Meyer, *J. Am. Chem. Soc.* **1982**, *104*, 4803 – 4810.

[14] E. Wachter, B. S. Howerton, E. C. Hall, S. Parkin, E. C. Glazer, *Chem. Commun.* **2014**, *50*, 311 – 313.

[15] E. Wachter, E. C. Glazer, *J. Phys. Chem. A* **2014**, *118*, 10474 – 10486.

[16] J. P. Hall, H. Beer, K. Buchner, D. J. Cardin, C. J. Cardin, *Philos. Trans. R. Soc. London Ser. A* **2013**, *371*, 20120525.

[17] a) E. J. C. Olson, D. Hu, A. Hormann, A. M. Jonkman, M. R. Arkin, E. D. A. Stemp, J. K. Barton, P. F. Barbara, *J. Am. Chem. Soc.* **1997**, *119*, 11458 – 11467; b) J. Olofsson, B. Önfelt, P. Lincoln, *J. Phys. Chem. A* **2004**, *108*, 4391 – 4398.

[18] In contrast, $[Ru(TAP)_2dppz\text{-}CH_3]^{2+}$ binds in a similar fashion to the previously mention complex except that the phenazine nitrogen is not solvent exposed; see J. P. Hall, H. Beer, K. Buchner, D. J. Cardin, C. J. Cardin, *Organometallics* **2015**, *34*, 2481 – 2486.

[19] A. W. McKinley, P. Lincoln, E. M. Tuite, *Coord. Chem. Rev.* **2011**, *255*, 2676 – 2692.

[20] Y. Wang, D. J. Patel, *Structure* **1993**, *1*, 263 – 282.

[21] G. N. Parkinson, M. P. H. Lee, S. Neidle, *Nature* **2002**, *417*, 876 – 880.

[22] a) Y. Xu, Y. Noguchi, H. Sugiyama, *Bioorg. Med. Chem.* **2006**, *14*, 5584 – 5591; b) A. Ambrus, D. Chen, J. Dai, T. Bialis, R. A. Jones, D. Yang, *Nucleic Acids Res.* **2006**, *34*, 2723 – 2735; c) K. N. Luu, A. T. Phan, V. Kuryavyi, L. Lacroix, D. J. Patel, *J. Am. Chem. Soc.* **2006**, *128*, 9963 – 9970.

[23] a) M. Vorlíčková, I. Kejnovská, J. Sagi, D. Renčiuk, K. Bednářová, J. Motlová, J. Kypr, *Methods* **2012**, *57*, 64 – 75; b) D. Renčiuk, I. Kejnovská, P. Školáková, K. Bednářová, J. Motlová, M. Vorlíčková, *Nucleic Acids Res.* **2009**, *37*, 6625 – 6634; c) J. Dai, M. Carver, D. Yang, *Biochimie* **2008**, *90*, 1172 – 1183.

[24] Our assignment is based upon ellipticity differences observed using circular dichroism when the DNA is folded in the presence of Na^+ and K^+ ions; the clear differences in these spectra support the characterization of the DNA folding into two disparate structures; see Figure S4 in the Supporting Information.

[25] a) I. Haq, P. Lincoln, D. C. Suh, B. Norden, B. Z. Chowdhry, J. B. Chaires, *J. Am. Chem. Soc.* **1995**, *117*, 4788 – 4796; b) F. G. Loontiens, P. Regenfuss, A. Zechel, L. Dumortier, R. M. Clegg, *Biochemistry* **1990**, *29*, 9029 – 9039.

[26] T. Wilson, P. J. Costa, V. Félix, M. P. Williamson, J. A. Thomas, *J. Med. Chem.* **2013**, *56*, 8674 – 8683.

[27] a) R. D. Gray, R. Buscaglia, J. B. Chaires, *J. Am. Chem. Soc.* **2012**, *134*, 16834 – 16844; b) T.-C. Chang, J.-F. Chu, Y.-L. Tsai, Z.-F. Wang, *Curr. Pharm. Des.* **2012**, *18*, 2002 – 2013; c) M. Bončina, J. Lah, I. Prislan, G. Vesnaver, *J. Am. Chem. Soc.* **2012**, *134*, 9657 – 9663; d) P. Stadlbauer, L. Trantírek, T. E. Cheatham III, J. Koča, J. Šponer, *Biochimie* **2014**, *105*, 22 – 35.

[28] E. Gavathiotis, R. A. Heald, M. F. Stevens, M. S. Searle, *J. Mol. Biol.* **2003**, *334*, 25 – 36.

[29] J. Dai, C. Punchihewa, A. Ambrus, D. Chen, R. A. Jones, D. Yang, *Nucleic Acids Res.* **2007**, *35*, 2440 – 2450.

[30] S. Shi, S. Gao, T. Cao, J. Liu, X. Gao, J. Hao, C. Lv, H. Huang, J. Xu, T. Yao, *PLoS One* **2013**, *8*, e84419.

[31] W. Paw, R. Eisenberg, *Inorg. Chem.* **1997**, *36*, 2287 – 2293.

[32] N. J. Lundin, P. J. Walsh, S. L. Howell, J. J. McGarvey, A. G. Blackman, K. C. Gordon, *Inorg. Chem.* **2005**, *44*, 3551 – 3560.

[33] R. M. Hartshorn, J. K. Barton, *J. Am. Chem. Soc.* **1992**, *114*, 5919 – 5925.

[34] APEX2, *Programs for data collection and data reduction*, Bruker-Nonius, Madison WI. USA, **2004**.

[35] G. M. Sheldrick, *SADABS & TWINABS*, University of Göttingen, Germany, **2008**.

[36] S. Parkin, B. Moezzi, H. Hope, *J. Appl. Crystallogr.* **1995**, *28*, 53 – 56.

[37] G. M. Sheldrick, *Acta Crystallogr. Sect. A* **2008**, *64*, 112 – 122.

[38] S. Parkin, *Acta Crystallogr. Sect. A* **2000**, *56*, 157 – 162.

[39] *International Tables for Crystallography, Vol C: Mathematical, Physical, and Chemical Tables*, Kluwer, Amsterdam, **1992**.

[40] Z. Otwinowski, W. Minor, *Processing of X-ray Diffraction Data Collected in Oscillation Mode*, *Methods Enzymol. Vol. 276*, **1997**.

Received: August 13, 2015
Published online on November 12, 2015